ORIGINAL ARTICLE

lajss.org© Latin American Journal of Solids and Structures

www.lajss.org

High frequency study functionally graded sandwich nanoplate with different skin layers resting on Pasternak foundation using higher-order IGA and nonlocal elasticity theory

Le Hoai[a], **Nhan Thinh Hoang**[b]*

[a]HUTECH Institute of Engineering, HUTECH University, Ho Chi Minh City, Viet Nam. Email: l.hoai@hutech.edu.vn
[b]Institute for Creative Design and Business, Nguyen Tat Thanh University, Ho Chi Minh City, Vietnam. Email: htnhan@ntt.edu.vn

* Corresponding author

https://doi.org/10.1590/1679-78258062

Abstract

For the first time, this article uses higher-order IGA to study the high frequency of the functionally graded sandwich (FGS) square nanoplates with two different skin layers resting on elastic foundations. In this work, the elastic foundations use the Pasternak foundation (PF) model with a two-parameter as a spring stiffness (k_1) and a shear layer stiffness (k_2). The observation of small-scale effects in nanoplates is accomplished by incorporating nonlocal elasticity theory (NET) with a higher-order shear deformation theory (HSDT). The governing equation of nanoplates is derived from Hamilton's principle. An extensive parametric investigation has been conducted to illustrate the free vibration characteristics of FGS square nanoplates across both low and high frequency modes, placing a greater emphasis on the analysis of high frequency behaviour. Furthermore, the high eigenmodes and frequencies of the FGS circular/elliptical nanoplates are also added. Therefore, the findings presented here contribute to an improved understanding of the vibrations of FGS nanoplates at high frequencies.

Keywords

Nanoplate, nonlocal elasticity theory, IGA, FGM, high frequency, free vibration.

Graphical Abstract

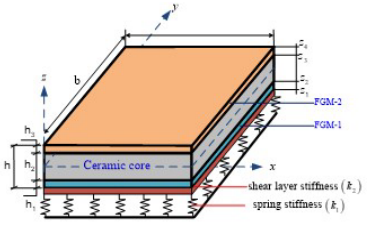

The FGS square nanoplate resting on PF

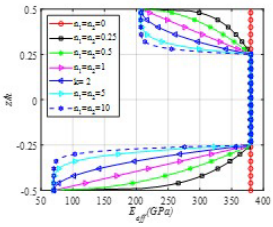

The effective elastic moduli via the nanoplate thickness.

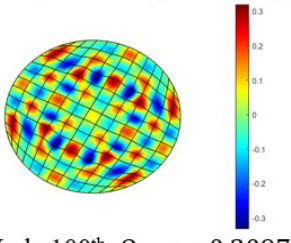

Mode 100th, $\Omega_{100} = 0.3097$

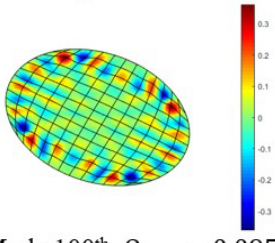

Mode 100th, $\Omega_{100} = 0.0951$

Received: February 24, 2024. In revised form: April 07, 2024. Accepted: April 22, 2024. Available online: May 03, 2024.
https://doi.org/https://doi.org/10.1590/1679-78258062

Nomenclature	
IGA	Isogeometric analysis
FEM	Finite element method
CPT	Classical plate theory
FSDT	First-order shear deformation theory
HSDT	Higher-order shear deformation theory
NSGT	Nonlocal strain gradient theory
SGT	Strain gradient theory
MCST	Modified couple stress theory
NET	Nonlocal elasticity theory
FGM	Functionally graded material
FGS	Functionally graded sandwich
BCs	Boundary conditions

1 INTRODUCTION

In recent years, nanostructures have become increasingly fascinating due to their distinct mechanical attributes and wide-ranging applications across various advanced engineering sectors. The basic forms of nanostructures, including nanobeams, nanoplates and nanoshells are of research interest in the field of nanoscale engineering (Ahmadi, 2022; Hadji, Avcar, & Civalek, 2021; Kachapi, 2020; Pham, Nguyen, Tran, & Nguyen-Thoi, 2021; Rouhi, Ansari, & Darvizeh, 2016; Zemri, Houari, Bousahla, & Tounsi, 2015). To gain a deeper understanding of their mechanical behaviour, a blend of experimental study and computer simulations has been utilized (Liew, He, & Wong, 2004; Stölken & Evans, 1998). However, this work is quite costly and time-consuming. Therefore, several theoretical models have been developed to explore nanostructures, such as NSGT Jiang, Li, and Hu (2023), SGT Toupin (1962), MCST Fleck and Hutchinson (1993), and NET Eringen (1984). These models are integrated with different shear deformation theories, encompassing CPTs, FSDTs, HSDTs, and quasi-3D theories to account for small-scale effects. Among these theories, NET combined with HSDT is often used due to its simple and highly accurate mathematical formulas.

Some typical studies on the mechanical behaviour of nanostructures include Aksencer and Aydogdu (2011) used an exact solution based on NET to analyze the vibration and buckling of nanoplates. (Ahmed Amine Daikh, Drai, Bensaid, Houari, & Tounsi, 2021; Daikh & Zenkour, 2020) employed Navier's solutions combined with NET and HSDT to study the thermal vibration and bending of FGS nanoplates. Shahverdi and Barati (2017) developed an exact method based on a comprehensive NSGT for vibration analysis of FG nanoplates. Arefi and Zenkour (2017) employed an exact solution based on a nonlocal HSDT to study the bending of sandwich nanoplates by the seven governing differential equations of the system. Sobhy and Radwan (2017) studied the buckling and vibration of FGM nanoplates using a new nonlocal quasi-3D. Luat et al. (2021) used a nonlocal closed-form solution to show the effect of dimension and material parameters on the bending, free vibration and buckling of FGM nanobeams. Hoa et al. (2021) used a one-variable shear deformation theory to examine the nonlocal behaviour of FGM nanoplates. Zhu, Fang, Liu, Nie, and Zhang (2022) employed a nonlocal Navier's solution to control the nonlinear vibration of FGS nanoshells. Thai, Ferreira, Nguyen-Xuan, Nguyen, and Phung-Van (2021) used a nonlocal mesh-free approach based on HSDT to conduct a mechanical analysis of nanoplates. In addition, Zeighampour and Shojaeian (2019) employed the Donnell shell theory based on MCST to examine the buckling of FGM nanoshells. It can be seen that previous studies often focused on analyzing the static, dynamic, and low frequency specific vibration behaviour of nanostructures. In engineering contexts, comprehending the dynamic reactions of nanostructures when subjected to high frequency loads is essential. These high frequency vibrations frequently occur in diverse micro/nano-electromechanical systems (MEMS/NEMS), nano-optomechanical devices, and resonators (Daneshmehr, Rajabpoor, & Hadi, 2015). Nanoplates and nanobeams are pivotal in crafting nanoscale sensors and actuators, where their steadfast operation amid high frequency stimulations is paramount. Delving into high frequency analyses yields crucial understandings of these structures' resonant tendencies and stability, facilitating tailored design optimization for distinct applications. Furthermore, such analyses assist in assessing the susceptibility to undesired vibrational modes, which could otherwise precipitate structural compromise or diminished functionality. It can be seen that there is an insufficient investigation of the influence of dimension parameters, material properties, and nonlocal factors on the high frequency behaviour of FGS nanoplates. So it motivated us to do this work to fill the above gap.

In addressing the limitations of classical FEM and exact solutions in structural analysis, (Borden, Scott, Evans, & Hughes, 2011; Hughes, Cottrell, & Bazilevs, 2005) introduced an advanced computational method known as IGA. This method seamlessly integrates Computer-Aided Design (CAD), offering a more robust and efficient approach to structural analysis. Using IGA helps to accurately describe the geometric domain as well as approximate unknown fields, so the number of variables does not increase. It is expected to yield more accurate results with lower computational costs in structural analysis Nguyen-Xuan, Tran, Thai, Kulasegaram, and Bordas (2014). Currently, IGA's open-source code can be

found on the Internet and in available resources (H. X. Nguyen et al., 2017; V. P. Nguyen, Anitescu, Bordas, & Rabczuk, 2015). With the above advantages, in recent years, the development and expansion of IGA to analyze the mechanical behaviour of structures (including nanostructures) have attracted the attention of many scientists. For example, Natarajan, Chakraborty, Thangavel, Bordas, and Rabczuk (2012) used IGA based on FSDT to analyze the nonlocal free vibration of FGM nanoplates. Cuong-Le, Nguyen, Lee, Rabczuk, and Nguyen-Xuan (2021) introduced a nonlocal 3D-IGA to examine the free vibration and buckling of multi-directional FGM nanoshells. Banh-Thien, Dang-Trung, Le-Anh, Ho-Huu, and Nguyen-Thoi (2017) employed nonlocal IGA for buckling analysis of variable-thickness nanoplates. Le and Tran (2023) employed non-polynomial higher-order IGA based on NET to study the dynamic response of honeycomb-FGS shells. In addition, (Ansari & Setoodeh, 2020; Ansari, Setoodeh & Rabczuk, 2020) also used IGA to discuss frequency loci veering and mode shape switching phenomena of FG blades with variable-thickness. The above studies have shown the superior convergence rate and accuracy of IGA compared to traditional FEM and analytical methods. Studies also show the suitability of IGA combined with HSDT and NET in analyzing the mechanical behaviour of nanostructures.

In this study, the authors use higher-order IGA combined with NET to analyze high frequency vibration of FGS nanoplates. The accuracy and reliability of the proposed method are confirmed by several comparative examples. Then, the influence of geometric parameters and material properties on the free vibration of FGS nanoplates is studied and described in detail, especially with high frequency vibrations. The obtained results are expected to contribute to calculating, designing, and optimizing nanoscale devices working at high frequencies.

2 PROBLEM MODEL AND ASSUMPTIONS

2.1 The FGS nanoplate model with different skin layers

In this study, the FGS square nanoplate with dimensions $a \times b \times h$ is considered. The sandwich nanoplate includes a ceramic core (Al2O3), the FGM-1 bottom layer (Al/Al2O3), and the FGM-2 top layer (Al2O3/SUS304) as presented in Fig. 1. A group of $h_1 - h_2 - h_3$ denotes the skin-core-skin ratio (so-called scheme) of FGS nanoplates with $h_1 = z_2 - z_1$, $h_2 = z_3 - z_2$, and $h_3 = z_4 - z_3$.

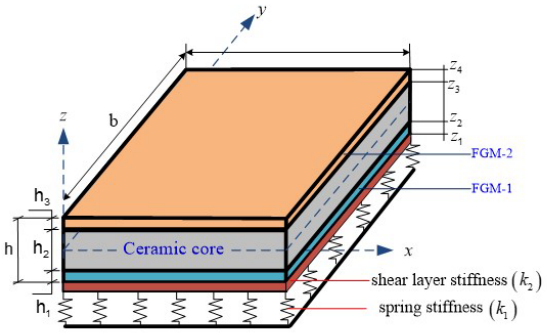

Figure 1 The FGS square nanoplate resting on PF.

The effective mechanical properties via thickness are defined by

$$\begin{cases} P(z) = P_b + (P_c - P_b)\left(\frac{z-z_1}{z_2-z_1}\right)^{n_1} & z \in [z_1; z_2] \\ P(z) = P_c & z \in [z_2; z_3] \\ P(z) = P_t + (P_c - P_t)\left(\frac{z-z_4}{z_3-z_4}\right)^{n_2} & z \in [z_3; z_4] \end{cases} \quad (1)$$

in which P_b, P_t, and P_c represent the mechanical properties such as elastic moduli, mass density, and Poisson's ratio of the bottom and top surfaces and the ceramic core layer of FGS nanoplates. n_1 and n_2 are the power-law indexes of FGM-1 and FGM-2, respectively. The mechanical properties are given in Table 1. The effective elastic moduli and mass density via the FGS nanoplate thickness (1-2-1) as plotted in Fig. 2.

Table 1 The mechanical properties of FGS nanoplates.

Materials	Elastic moduli (GPa)	Mass density (kg/m^3)	Poisson's ratio
Al	70	2707	0.3
Al_2O_3	380	3800	0.3
SUS304	207	8166	0.3
Si_3N_4	348.43	2370	0.3

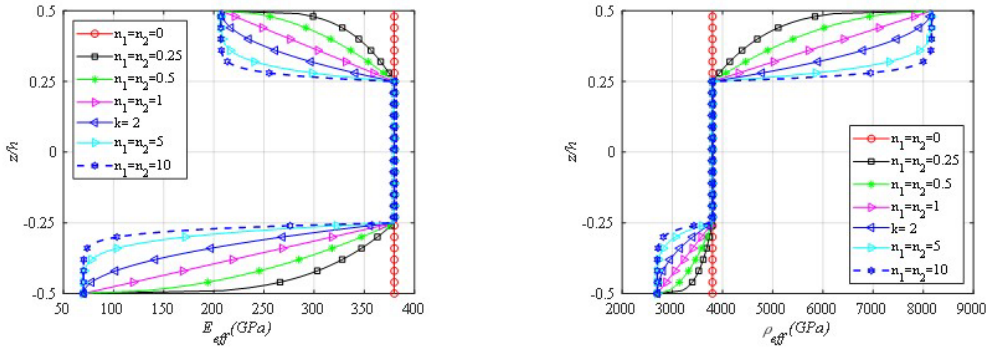

a) Elastic moduli. b) The mass density.

Figure 2 The effective mechanical properties via the nanoplate thickness.

2.2 Pasternak foundation

The PF is two-parameter model (k_1, k_2) that describes the foundation reaction as a function of the deflection and its Laplacian. The reaction-deflection relation of PF is defined by Shahsavari, Shahsavari, Li, and Karami (2018):

$$\mathcal{R} = k_1 w(x,y) - k_2 \left(\frac{\partial^2}{\partial x^2} + \frac{\partial^2}{\partial y^2}\right) w(x,y) \tag{2}$$

3 THEORETICAL FORMULATION

3.1 Nonlocal elasticity theory

According to Eringen's NET (Eringen, 1984), the stress field is determined by:

$$(1 - \mu\nabla^2)\boldsymbol{\sigma} = \boldsymbol{\sigma}^l \tag{3}$$

herein $\boldsymbol{\sigma}^l$ is the local stress tensor, μ denotes the small-scale effect (nonlocal factor), and $\nabla^2 = \frac{\partial^2}{\partial x^2} + \frac{\partial^2}{\partial y^2}$ is the Laplacian operator. Note that $\mu = 0$ corresponds to local plate theory.

3.2 The higher-order shear deformation theory

Following HSDT (Sobhy, 2016), the displacement field of FGS nanoplates is expressed by

$$\begin{cases} u(x,y,z) = u_0(x,y) - z\dfrac{\partial w}{\partial x} + f(z)\varphi_x \\ v(x,y,z) = v_0(x,y) - z\dfrac{\partial w}{\partial y} + f(z)\varphi_y \\ \qquad w(x,y,z) = w_0(x,y). \end{cases} \tag{4}$$

where u_0, v_0, φ_x, φ_y, and w_0 are displacement variables. $f(z) = z/(1 + 4z^2/h^2)$ is Touratier's transverse shear function (Touratier, 1991).

The strain-displacement relations are determined by

$$\boldsymbol{\varepsilon} = \boldsymbol{\varepsilon}_0^{\square} + z\boldsymbol{\kappa}_1 + f(z)\boldsymbol{\kappa}_2 \tag{5a}$$

$$\boldsymbol{\gamma} = f'(z)\boldsymbol{\kappa}_3 \tag{5b}$$

with the symbol "′" is the derivative with respect to the variable z.

and

$$\boldsymbol{\varepsilon}_0^{\square} = \begin{Bmatrix} u_{0,x} \\ v_{0,y} \\ u_{0,y} + v_{0,x} \end{Bmatrix}; \boldsymbol{\kappa}_1 = -2\begin{Bmatrix} 0.5w_{,xx} \\ 0.5w_{,yy} \\ w_{,xy} \end{Bmatrix}; \boldsymbol{\kappa}_2 = -2\begin{Bmatrix} \varphi_{x,x} \\ \varphi_{y,y} \\ \varphi_{x,y} + \varphi_{y,x} \end{Bmatrix}; \boldsymbol{\kappa}_3 = \begin{Bmatrix} \varphi_x \\ \varphi_y \end{Bmatrix} \tag{6}$$

The local stress resultants are defined by

$$[\mathbb{N}^l;\ \mathcal{M}^l;\ \wp^l] = \mathbb{Q}_1\left[\boldsymbol{\varepsilon}_0^{\square};\ \boldsymbol{\kappa}_1;\ \boldsymbol{\kappa}_2\right];\ \mathrm{Q}^l = \mathbb{Q}_2\boldsymbol{\kappa}_3 \tag{7}$$

Where

$$\mathbb{Q}_1 = \begin{bmatrix} \mathbb{A} & \mathbb{B} & \mathbb{B}^b \\ \mathbb{B} & \mathbb{F} & \mathbb{F}^b \\ \mathbb{B}^b & \mathbb{F}^b & \mathbb{H} \end{bmatrix}; \mathbb{Q}_2 = \int_{\frac{-h}{2}}^{\frac{h}{2}} \frac{E(z)}{2(1+\nu(z))}\begin{bmatrix} 1 & 0 \\ 0 & 1 \end{bmatrix}\left(f'(z)\right)^2 dz \tag{8}$$

with $\mathbb{A}, \mathbb{B}, \mathbb{B}^b, \mathbb{F}, \mathbb{F}^b, \mathbb{H}$ are computed by

$$(\mathbb{A}, \mathbb{B}, \mathbb{B}^b, \mathbb{F}, \mathbb{F}^b, \mathbb{H}) = \int_{\frac{-h}{2}}^{\frac{h}{2}} \frac{E(z)}{1-\nu(z)^2}\begin{bmatrix} 1 & \nu(z) & 0 \\ \nu(z) & 1 & 0 \\ 0 & 0 & \frac{1}{2(1-\nu(z))} \end{bmatrix}(1, z, z^2, f(z), zf(z), f^2(z))dz; \tag{9}$$

Now, Eq. (3) is rewritten in matrix form as follows:

$$\begin{Bmatrix} \mathbb{N} \\ \mathcal{M} \\ \wp \\ \mathrm{Q} \end{Bmatrix} - \mu\nabla^2\begin{Bmatrix} \mathbb{N} \\ \mathcal{M} \\ \wp \\ \mathrm{Q} \end{Bmatrix} = \begin{bmatrix} \mathbb{A} & \mathbb{B} & \mathbb{B}^b & 0 \\ \mathbb{B} & \mathbb{F} & \mathbb{F}^b & 0 \\ \mathbb{B}^b & \mathbb{F}^b & \mathbb{H} & 0 \\ 0 & 0 & 0 & \mathbb{Q}_2 \end{bmatrix}\begin{Bmatrix} \boldsymbol{\varepsilon}_{\boldsymbol{m}}^{\square} \\ \boldsymbol{\kappa}_1 \\ \boldsymbol{\kappa}_2 \\ \boldsymbol{\kappa}_3 \end{Bmatrix} \tag{10}$$

The governing equation for the free vibration of nanoplates is derived from Hamilton's principle as follows Reddy (2006):

$$\int_0^T\left(\delta U + \delta U^f - \delta T\right)dt = 0. \tag{11}$$

in which δU, δU^f and δT denote the virtual strain energy, the virtual deformed foundation and the virtual kinetic energy, respectively. They are defined by

$$\delta U = \int_{\mathrm{S}}^{\square}\left(\left(\delta\boldsymbol{\varepsilon}_0^{\square}\right)^T\mathbb{N} + (\delta\boldsymbol{\kappa}_1)^T\mathcal{M} + (\delta\boldsymbol{\kappa}_2)^T\wp + (\delta\boldsymbol{\kappa}_3)^T\mathrm{Q}\right)dS. \tag{12}$$

$$\delta U^f = \int_{\mathrm{S}}^{\square}\mathcal{R}\delta w\,\mathrm{Ds} \tag{13}$$

$$\delta T = \int_{\mathrm{v}}^{\square}\rho(z)(\dot{u}\delta\dot{u} + \dot{v}\delta\dot{v} + \dot{w}\delta\dot{w})\,dxdydz = \int_{\mathrm{S}}^{\square}(\delta\dot{\boldsymbol{u}}_1^T\boldsymbol{\ell}\dot{\boldsymbol{u}}_1 + \delta\dot{\boldsymbol{u}}_2^T\boldsymbol{\ell}\dot{\boldsymbol{u}}_2 + \delta\dot{\boldsymbol{u}}_3^T\boldsymbol{\ell}\dot{\boldsymbol{u}}_3)\,dxdy = \int_{\mathrm{S}}^{\square}\delta\dot{\boldsymbol{u}}^T\mathcal{L}\dot{\boldsymbol{u}}\,dS \tag{14}$$

where ρ is the mass density and Φ is the inertial matrix defined by

$$\mathcal{L} = \begin{bmatrix} \boldsymbol{\ell} & 0 & 0 \\ 0 & \boldsymbol{\ell} & 0 \\ 0 & 0 & \boldsymbol{\ell} \end{bmatrix} \tag{15}$$

in there

$$\boldsymbol{\ell} = \begin{bmatrix} m_0 & m_1 & m_f \\ m_1 & m_2 & m_{zf} \\ m_f & m_{zf} & m_{ff} \end{bmatrix} \tag{16}$$

With

$$\left(m_0, m_1, m_2, m_f, m_{zf}, m_{ff}\right) = \int_{\frac{-h}{2}}^{\frac{h}{2}} \rho(1, z, z^2, f(z), zf(z), f^2(z)) dz \tag{17a}$$

And

$$\boldsymbol{u} = \begin{Bmatrix} \boldsymbol{u}_1 \\ \boldsymbol{u}_2 \\ \boldsymbol{u}_3 \end{Bmatrix};\ \boldsymbol{u}_1 = \begin{Bmatrix} u_0 \\ -w_{,x} \\ \varphi_x \end{Bmatrix};\ \boldsymbol{u}_2 = \begin{Bmatrix} v_0 \\ -w_{,y} \\ \varphi_y \end{Bmatrix};\ \boldsymbol{u}_3 = \begin{Bmatrix} w \\ 0 \\ 0 \end{Bmatrix};\ \dot{\boldsymbol{u}}_1 = \begin{Bmatrix} \dot{u}_0 \\ -\dot{w}_{,x} \\ \dot{\varphi}_x \end{Bmatrix};\ \dot{\boldsymbol{u}}_2 = \begin{Bmatrix} \dot{v}_0 \\ -\dot{w}_{,y} \\ \dot{\varphi}_y \end{Bmatrix};\ \dot{\boldsymbol{u}}_3 = \begin{Bmatrix} \dot{w} \\ 0 \\ 0 \end{Bmatrix}. \tag{17b}$$

The weak form for the free vibration of nanoplates is determined by Reddy (2006):

$$\int_S ((\delta\boldsymbol{\varepsilon})^T \mathbb{Q}_1 \delta\boldsymbol{\varepsilon} + (\delta\boldsymbol{\kappa}_3)^T \mathbb{Q}_2 \delta\boldsymbol{\kappa}_3)\, dS + \int_S (1 - \mu\nabla^2)\mathcal{R}\delta w \, dS + \int_S \delta\boldsymbol{u}^T (1 - \mu\nabla^2)\Phi\ddot{\boldsymbol{u}}\, dS = 0 \tag{18}$$

3.3 Isogeometric analysis

IGA based on NURBS basis functions to estimate the displacement field. An inherent benefit of IGA lies in its capacity to accommodate varying degrees of smoothness through the adjustment of interpolation orders, facilitating the fulfillment of continuity requirements as per HSDT. Furthermore, it is noteworthy that the integration of higher-order IGA with NET is regarded as the most efficient analytical approach for nanoplates.

The displacement field of plates is defined by Hughes, et al. (2005):

$$\boldsymbol{u}(\xi, \eta) = \begin{Bmatrix} u_0 \\ v_0 \\ w_0 \\ \varphi_x \\ \varphi_y \end{Bmatrix} = \sum_{K=1}^{m \times n} \begin{bmatrix} R_K(\xi,\eta) & 0 & 0 & 0 & 0 \\ 0 & R_K(\xi,\eta) & 0 & 0 & 0 \\ 0 & 0 & R_K(\xi,\eta) & 0 & 0 \\ 0 & 0 & 0 & R_K(\xi,\eta) & 0 \\ 0 & 0 & 0 & 0 & R_K(\xi,\eta) \end{bmatrix} \boldsymbol{d}_K \tag{19}$$

with the displacement vector $\boldsymbol{d}_K = \{u_{0K}\ v_{0K}\ w_{0K}\ \varphi_{xK}\ \varphi_{yK}\}^T$ associate with control point K and R_K is the shape function (Borden, et al., 2011).

Substituting Eq. (19) into Eq. (6), the strain field is obtained as follows:

$$\left[\boldsymbol{\varepsilon}_m;\ \boldsymbol{\kappa}_1;\ \boldsymbol{\kappa}_2;\ \boldsymbol{\kappa}_3\right] = \sum_{K=1}^{m \times n} \left[\boldsymbol{B}_m;\ \boldsymbol{B}_1;\ \boldsymbol{B}_2;\ \boldsymbol{B}_3\right] \boldsymbol{d}_K \tag{20}$$

in which

$$\boldsymbol{B}_m = \begin{bmatrix} \boldsymbol{R}_{K,x} & 0 & 0 & 0 & 0 \\ 0 & \boldsymbol{R}_{K,y} & 0 & 0 & 0 \\ \boldsymbol{R}_{K,y} & \boldsymbol{R}_{K,x} & 0 & 0 & 0 \end{bmatrix} \tag{21a}$$

$$\boldsymbol{B}_1 = \begin{bmatrix} 0 & 0 & -\boldsymbol{R}_{K,xx} & 0 & 0 \\ 0 & 0 & -\boldsymbol{R}_{K,yy} & 0 & 0 \\ 0 & 0 & -2\boldsymbol{R}_{K,xy} & 0 & 0 \end{bmatrix} \tag{21b}$$

$$\boldsymbol{B}_2^{\square} = \begin{bmatrix} 0 & 0 & 0 & \boldsymbol{R}_{K,x} & 0 \\ 0 & 0 & 0 & 0 & \boldsymbol{R}_{K,y} \\ 0 & 0 & 0 & \boldsymbol{R}_{K,y} & \boldsymbol{R}_{K,x} \end{bmatrix} \tag{21c}$$

$$\boldsymbol{B}_3^{\square} = \begin{bmatrix} 0 & 0 & 0 & \boldsymbol{R}_K & 0 \\ 0 & 0 & 0 & 0 & \boldsymbol{R}_K \end{bmatrix} \tag{21d}$$

Substituting Eq. (20) into Eq. (18), the equation for the free vibration of nanoplates is:

$$\boldsymbol{M}\ddot{\boldsymbol{d}} + \left(\boldsymbol{K} + \boldsymbol{K}_{\square}^{f}\right)\boldsymbol{d} = \boldsymbol{0} \tag{22}$$

The assumption that $\boldsymbol{u} = \boldsymbol{u}_0\, sin(\omega t) \neq 0$, we have:

$$\left|\left(\boldsymbol{K} + \boldsymbol{K}_{\square}^{f}\right) - \omega^2 \boldsymbol{M}\right| = \boldsymbol{0} \tag{23}$$

with ω is the natural frequency.

The stiffness matrix is:

$$\boldsymbol{K} = \int_{\mathrm{S}}^{\square} \left(\begin{bmatrix} \boldsymbol{B}_m \\ \boldsymbol{B}_1 \\ \boldsymbol{B}_2 \end{bmatrix}^T \underbrace{\begin{bmatrix} \mathbb{A} & \mathbb{B} & \mathbb{B}^b \\ \mathbb{B} & \mathbb{F} & \mathbb{F}^b \\ \mathbb{B}^b & \mathbb{F}^b & \mathbb{H} \end{bmatrix}}_{\mathbb{Q}_1} \begin{bmatrix} \boldsymbol{B}_m \\ \boldsymbol{B}_1 \\ \boldsymbol{B}_2 \end{bmatrix} + (\boldsymbol{B}_3)^T \mathbb{Q}_2 \boldsymbol{B}_3 \right) dS \tag{24}$$

The foundation stiffness matrix is:

$$\boldsymbol{K}_{\square}^{f} = k_1 \int_{\mathrm{S}}^{\square} \left[(\boldsymbol{R}_K)^{\mathrm{T}} (\boldsymbol{R}_K) \mathrm{dS} + \mu[\left(\boldsymbol{R}_{K,x}\right)^{\mathrm{T}} \left(\boldsymbol{R}_{K,x}\right) + \left(\boldsymbol{R}_{K,y}\right)^{\mathrm{T}} \left(\boldsymbol{R}_{K,y}\right)] \right] \mathrm{dS} + \mathrm{k}_2 \int_{\mathrm{S}}^{\square} \left[\left(\boldsymbol{R}_{K,x}\right)^{\mathrm{T}} \left(\boldsymbol{R}_{K,x}\right) + \left(\boldsymbol{R}_{K,y}\right)^{\mathrm{T}} \left(\boldsymbol{R}_{K,y}\right) + \mu[\left(\boldsymbol{R}_{K,xx}\right)^{\mathrm{T}} \left(\boldsymbol{R}_{K,xx}\right) + \left(\boldsymbol{R}_{K,yy}\right)^{\mathrm{T}} \left(\boldsymbol{R}_{K,yy}\right) + \left(\boldsymbol{R}_{K,xx}\right)^{\mathrm{T}} \left(\boldsymbol{R}_{K,yy}\right) + \left(\boldsymbol{R}_{K,yy}\right)^{\mathrm{T}} \left(\boldsymbol{R}_{K,xx}\right)] \right] \mathrm{dS} \tag{25}$$

The mass matrix is:

$$\boldsymbol{M} = \int_{\mathrm{S}}^{\square} \begin{bmatrix} \boldsymbol{X}_1 \\ \boldsymbol{X}_2 \\ \boldsymbol{X}_3 \end{bmatrix}^T \left(\underbrace{\begin{bmatrix} \boldsymbol{\ell} & 0 & 0 \\ 0 & \boldsymbol{\ell} & 0 \\ 0 & 0 & \boldsymbol{\ell} \end{bmatrix}}_{\hat{\mathcal{L}}} - \mu \nabla^2 \underbrace{\begin{bmatrix} \boldsymbol{\ell} & 0 & 0 \\ 0 & \boldsymbol{\ell} & 0 \\ 0 & 0 & \boldsymbol{\ell} \end{bmatrix}}_{\hat{\mathcal{L}}} \right) \begin{bmatrix} \boldsymbol{X}_1 \\ \boldsymbol{X}_2 \\ \boldsymbol{X}_3 \end{bmatrix} dS \tag{26}$$

With

$$\boldsymbol{X}_1^{\square} = \begin{bmatrix} \boldsymbol{R}_K & 0 & 0 & 0 & 0 \\ 0 & 0 & -\boldsymbol{R}_{K,x} & 0 & 0 \\ 0 & 0 & 0 & \boldsymbol{R}_K & 0 \end{bmatrix} \tag{27a}$$

$$\boldsymbol{X}_2^{\square} = \begin{bmatrix} 0 & \boldsymbol{R}_K & 0 & 0 & 0 \\ 0 & 0 & -\boldsymbol{R}_{K,y} & 0 & 0 \\ 0 & 0 & 0 & 0 & \boldsymbol{R}_K \end{bmatrix} \tag{27b}$$

$$\boldsymbol{X}_3^{\square} = \begin{bmatrix} 0 & 0 & \boldsymbol{R}_K & 0 & 0 \\ 0 & 0 & 0 & 0 & 0 \\ 0 & 0 & 0 & 0 & 0 \end{bmatrix} \tag{27c}$$

In this study, the BCs are given by

- Clamped (C): $u_0 = v_0 = w_0 = \varphi_x = \varphi_y = 0$ at all edges.
- Simply supported (S): $u_0 = w_0 = \varphi_x = 0$ at $y = 0$ & $y = b$; $v_0 = w_0 = \varphi_y = 0$ at $x = 0$ & $x = a$.

4 NUMERICAL RESULTS

This section is done for the following two purposes: (i) verifying the convergence and performance of the proposed method; (ii) analyzing the influence of input parameters on the free vibration of FGS nanoplates including low and high frequency.

4.1 Verification

Firstly, the dimensionless frequencies $\omega^* = 10\omega h\sqrt{\rho_b/E_b}$ of the SSSS SUS304/Si_3N_4 square nanoplates are listed in Table 2. Observing that the obtained results converge with a mesh size of 9×9, and are close to those of exact solutions using quasi-3D theory (Sobhy & Radwan, 2017) and HSDT (Ahmed Amine Daikh, et al., 2021). From the comparison results, the accuracy and reliability of the present method can be confirmed. Furthermore, the convergence study at high frequencies is shown in Fig. 3. It can be seen that the high frequencies change little at the mesh size of 11x11. Therefore, to enhance the smoothness of the deformation field and ensure accuracy, a mesh size of 13x13 is used for the following examples.

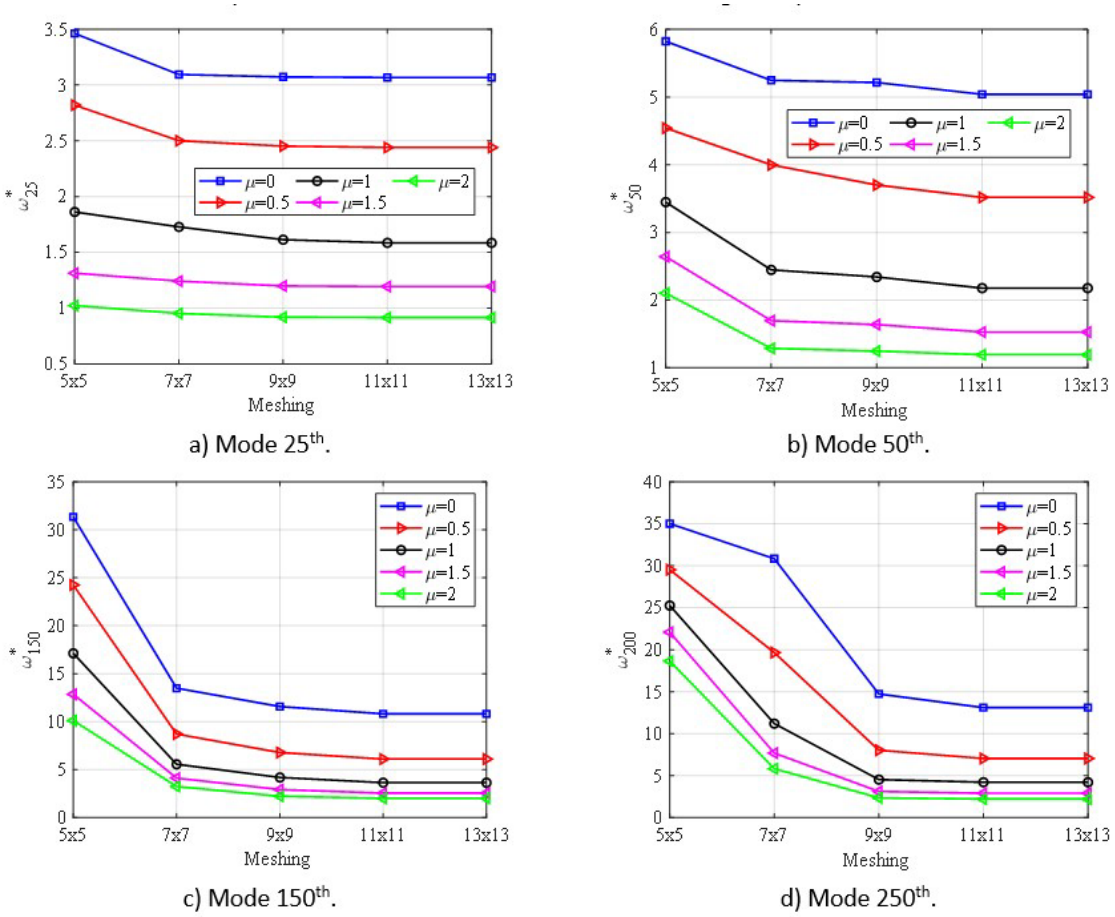

Figure 3 High frequency of nanoplates with different mesh sizes.

Secondly, let us consider the SSSS FGM (Al/Al_2O_3) plate with $h = a/20$ resting on PF. The dimensionless formulas are defined by

$$K_1 = \frac{k_1 a^4}{H_b}; K_2 = \frac{k_2 a^2}{H_b} with\ H_b = \frac{E_b h^3}{12(1-\upsilon^2)};\ \Omega = \omega h\sqrt{\frac{\rho_b}{E_b}} \tag{28}$$

It can be observed that the achieved outcomes are in good agreement with those of exact solutions utilizing a novel hyperbolic quasi-3D theory (Shahsavari, et al., 2018) and TSDT (Baferani, Saidi, & Ehteshami, 2011), as given in Table 3. The maximum error is approximately 3%. This example further strengthens the reliability of the present method.

Table 2 Comparison of the first frequencies of SSSS FGM nanoplates ($n = 1$).

$\frac{a}{h}$	Method	Mesh size	Nonlocal factor				
			$\mu = 0$	$\mu = 0.5$	$\mu = 1$	$\mu = 1.5$	$\mu = 2$
10	Present	5×5	0.82335	0.80376	0.75243	0.68514	0.61548
		7×7	0.82331	0.80372	0.75240	0.68511	0.61545
		9×9	0.82330	0.80371	0.75239	0.68510	0.61544
		11×11	0.82330	0.80371	0.75239	0.68510	0.61544
		13×13	0.82330	0.80371	0.75239	0.68510	0.61544
	Sobhy and Radwan (2017)		0.82250	0.80292	0.75165	0.68443	0.61484
	Ahmed Amine Daikh, et al. (2021)		0.82296	0.80338	0.75208	0.68483	0.61520
20	Present	5×5	0.20970	0.20471	0.19164	0.17450	0.15676
		7×7	0.20969	0.20470	0.19163	0.17449	0.15675
		9×9	0.20969	0.20470	0.19163	0.17449	0.15675
		11×11	0.20969	0.20470	0.19162	0.17449	0.15675
		13×13	0.20969	0.20470	0.19162	0.17449	0.15675
	Sobhy and Radwan (2017)		0.21083	0.20581	0.19267	0.17544	0.15760
	Ahmed Amine Daikh, et al. (2021)		0.21098	0.20596	0.19280	0.17556	0.15771

Table 3 Comparison of the first frequencies of FGM plates resting on PF.

(K_1, K_2)	n	Present	Shahsavari, et al. (2018)		Baferani, et al. (2011)	
			Ω	Error (%)	Ω	Error (%)
(0, 0)	0	0.0292	0.0290	0.69	0.0291	0.34
	1	0.0223	0.0227	1.76	0.0226	1.33
	2	0.0202	0.0209	3.35	0.0206	1.94
	5	0.0191	0.0197	3.05	0.0195	2.05
(100, 0)	0	0.0299	0.0298	0.34	0.0298	0.34
	1	0.0233	0.0238	2.10	0.0236	1.27
	2	0.0214	0.0221	3.17	0.0218	1.83
	5	0.0205	0.0210	2.38	0.0208	1.44
(100, 100)	0	0.0412	0.0411	0.24	0.0411	0.24
	1	0.0385	0.0388	0.77	0.0386	0.26
	2	0.0381	0.0386	1.30	0.0383	0.52
	5	0.0384	0.0388	1.03	0.0385	0.26

Note that: $\text{Error } (\%) = 100 \times \frac{|\Omega_{pr} - \Omega_{re}|}{|\Omega_{re}|}$ with Ω_{pr} and Ω_{re} dimensionless frequencies of the present and reference, respectively.

4.2 The high frequency of FGS nanoplates

In this part, the authors focus on the study of an FGS square nanoplate with $a = b = 10$ nm. The dimensionless formulas are given by Eq. (28) with E_b and ρ_b are replaced by E_{Al} and ρ_{Al}. The meshing with the detail of the knots and control points is shown in Fig. 4.

Firstly, the first frequencies of FGS square nanoplates with different values of schemes, power-law indexes, BCs, and nonlocal factors are listed in Table 4. The first six frequencies of the FGS nanoplates (1-2-1) are shown in Table 5. Observing that the increase in the power-law indexes ($n_1 = n_2$) and nonlocal factor μ reduces the FGS nanoplate stiffness leading to a decrease in the frequency of FGS nanoplates, as expected. Besides, the thicker ceramic core results in a stiffer nanoplate, causing the frequency of the FGS nanoplate to increase correspondingly 1-0-1, 1-1-1, 1-2-2, 1-2-1, 1-4-1, and 1-6-1. Furthermore, with the same geometry and material parameters, simply supported nanoplates are softer resulting in smaller frequencies than tightly clamped nanoplates.

Secondly, the six frequencies of FGS square nanoplates (1-4-1) from the 20th mode to the 25th mode are listed in Table 6 and the frequencies of FGS square nanoplates (1-6-1) from the 150th mode to the 155th mode are listed in Table 7. Observing that the frequency of FGS square nanoplates with $n_1 = n_2 = 0$ is the highest because when $n_1 = n_2 = 0$, the FGS square nanoplate becomes rich-ceramic nanoplate. It can be seen that, as the nonlocal factors intensify, the frequencies of FGS square nanoplates across all mode sequence numbers exhibit a decrease. A thorough examination of these tables indicates that the influence of nonlocal factors is more pronounced on higher frequencies compared to their effect on the lower frequencies of FGS square nanoplates.

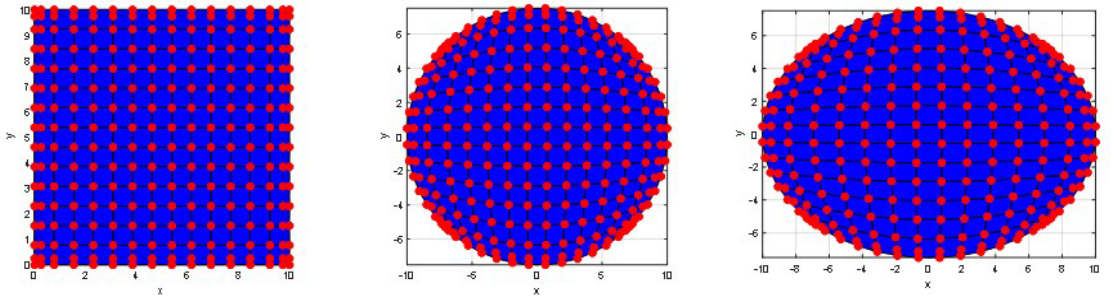

a) The meshing of 13 × 13 cubic NURBS element (Rectangular nanoplate)

b) The meshing of 13 × 13 cubic NURBS element (Circular nanoplate)

c) The meshing of 13 × 13 cubic NURBS element (Elliptical nanoplate)

Figure 4 Control net of FGS nanoplates.

Table 4 The first frequencies of FGS nanoplates with $a/h = 10, K_1 = 100, K_2 = 10$.

BCs	$n_1 = n_2$	μ	Schemes					
			1-0-1	1-1-1	1-2-2	1-2-1	1-4-1	1-6-1
SSSS	0	0	0.1223	0.1223	0.1223	0.1223	0.1223	0.1223
		0.5	0.1174	0.1174	0.1174	0.1174	0.1174	0.1174
		1.5	0.1095	0.1095	0.1095	0.1095	0.1095	0.1095
		2.5	0.1032	0.1032	0.1032	0.1032	0.1032	0.1032
		4.0	0.0960	0.0960	0.0960	0.0960	0.0960	0.0960
	1	0	0.0844	0.0924	0.0940	0.0980	0.1046	0.1087
		0.5	0.0814	0.0890	0.0905	0.0943	0.1006	0.1045
		1.5	0.0765	0.0835	0.0848	0.0884	0.0941	0.0977
		2.5	0.0728	0.0792	0.0803	0.0837	0.0890	0.0923
		4.0	0.0684	0.0743	0.0752	0.0784	0.0831	0.0861
	2.5	0	0.0727	0.0818	0.0845	0.0889	0.0975	0.1035
		0.5	0.0703	0.0789	0.0814	0.0857	0.0939	0.0995
		1.5	0.0664	0.0743	0.0765	0.0805	0.0880	0.0931
		2.5	0.0634	0.0707	0.0726	0.0765	0.0834	0.0881
		4.0	0.0600	0.0666	0.0682	0.0718	0.0780	0.0823
	9.5	0	0.0658	0.0743	0.0776	0.0823	0.0921	0.1003
		0.5	0.0638	0.0718	0.0749	0.0795	0.0887	0.0965
		1.5	0.0605	0.0679	0.0705	0.0749	0.0833	0.0904
		2.5	0.0579	0.0648	0.0671	0.0713	0.0790	0.0856
		4.0	0.0550	0.0613	0.0632	0.0671	0.0741	0.0800
CCCC	0	0	0.2012	0.2012	0.2012	0.2012	0.2012	0.2012
		0.5	0.1916	0.1916	0.1916	0.1916	0.1916	0.1916
		1.5	0.1761	0.1761	0.1761	0.1761	0.1761	0.1761
		2.5	0.1643	0.1643	0.1643	0.1643	0.1643	0.1643
		4.0	0.1510	0.1510	0.1510	0.1510	0.1510	0.1510
	1	0	0.1366	0.1509	0.1539	0.1605	0.1717	0.1786
		0.5	0.1306	0.1440	0.1468	0.1531	0.1637	0.1702
		1.5	0.1211	0.1332	0.1356	0.1414	0.1509	0.1569
		2.5	0.1139	0.1250	0.1271	0.1325	0.1413	0.1467
		4.0	0.1059	0.1158	0.1175	0.1225	0.1303	0.1352
	4	0	0.1091	0.1258	0.1318	0.1392	0.1551	0.1667
		0.5	0.1048	0.1204	0.1260	0.1330	0.1481	0.1590
		1.5	0.0979	0.1120	0.1168	0.1234	0.1369	0.1467
		2.5	0.0928	0.1057	0.1099	0.1160	0.1284	0.1374
		4.0	0.0870	0.0986	0.1021	0.1078	0.1189	0.1269
	10	0	0.1025	0.1186	0.1252	0.1331	0.1502	0.1642
		0.5	0.0985	0.1137	0.1197	0.1273	0.1434	0.1566
		1.5	0.0923	0.106	0.1112	0.1182	0.1327	0.1446
		2.5	0.0876	0.1001	0.1047	0.1113	0.1246	0.1355
		4.0	0.0825	0.0937	0.0974	0.1036	0.1154	0.1252

Table 5 The first six frequencies of FGS nanoplates (1-2-1) with $a/h = 20, K_1 = 50, K_2 = 15$.

BCs	$n_1 = n_2$	μ	The first six dimensionless frequencies					
			Ω_1	Ω_2	Ω_3	Ω_4	Ω_5	Ω_6
SSSS	0	0	0.0315	0.0740	0.0745	0.1163	0.1428	0.1453
		1	0.0292	0.0615	0.0618	0.0882	0.1028	0.1046
		2	0.0274	0.0540	0.0544	0.0745	0.0852	0.0867
		3	0.0260	0.0490	0.0493	0.0661	0.0749	0.0762
		4	0.0248	0.0453	0.0456	0.0603	0.0679	0.0691
	1	0	0.0252	0.0582	0.0586	0.0912	0.1118	0.1140
		1	0.0235	0.0486	0.0489	0.0696	0.0810	0.0826
		2	0.0221	0.0430	0.0433	0.0592	0.0676	0.0689
		3	0.0211	0.0392	0.0395	0.0528	0.0597	0.0609
		4	0.0203	0.0365	0.0367	0.0484	0.0545	0.0555
	2	0	0.0233	0.0534	0.0538	0.0836	0.1024	0.1045
		1	0.0218	0.0448	0.0451	0.0640	0.0745	0.0760
		2	0.0206	0.0397	0.0400	0.0546	0.0623	0.0636
		3	0.0197	0.0363	0.0366	0.0488	0.0552	0.0563
		4	0.0189	0.0338	0.0341	0.0449	0.0505	0.0515
	10	0	0.0211	0.0478	0.0482	0.0746	0.0913	0.0931
		1	0.0198	0.0402	0.0405	0.0574	0.0667	0.0680
		2	0.0188	0.0358	0.0361	0.0491	0.0560	0.0572
		3	0.0180	0.0329	0.0331	0.0441	0.0499	0.0509
		4	0.0174	0.0308	0.0310	0.0407	0.0457	0.0467
SCSC	0	0	0.0440	0.0812	0.1014	0.1365	0.1472	0.1844
		1	0.0405	0.0671	0.0827	0.1022	0.1056	0.1303
		2	0.0378	0.0588	0.0720	0.0859	0.0875	0.1069
		3	0.0357	0.0533	0.0650	0.0760	0.0768	0.0928
		4	0.0340	0.0492	0.0599	0.0692	0.0697	0.0837
	0.5	0	0.0377	0.0694	0.0867	0.1167	0.1256	0.1580
		1	0.0348	0.0575	0.0710	0.0877	0.0905	0.1121
		2	0.0326	0.0506	0.0620	0.0740	0.0752	0.0921
		3	0.0309	0.0460	0.0562	0.0657	0.0663	0.0803
		4	0.0295	0.0427	0.0519	0.0600	0.0603	0.0726
	1.5	0	0.0331	0.0606	0.0757	0.1018	0.1094	0.1379
		1	0.0307	0.0505	0.0622	0.0769	0.0792	0.0983
		2	0.0288	0.0446	0.0546	0.0651	0.0661	0.0811
		3	0.0274	0.0407	0.0496	0.058	0.0585	0.0709
		4	0.0263	0.0378	0.046	0.0532	0.0534	0.0644
	8.5	0	0.0289	0.0526	0.0656	0.0882	0.0947	0.1196
		1	0.0269	0.0441	0.0543	0.0670	0.0690	0.0857
		2	0.0255	0.0391	0.0479	0.0571	0.0579	0.0710
		3	0.0243	0.0359	0.0437	0.0511	0.0515	0.0625
		4	0.0234	0.0335	0.0408	0.0471	0.0472	0.0569

Table 6 The six frequencies of FGS square nanoplates (1-4-1) with $a/h = 25, K_1 = 75, K_2 = 50$.

BCs	$n_1 = n_2$	μ	The six dimensionless frequencies					
			Ω_{20}	Ω_{21}	Ω_{22}	Ω_{23}	Ω_{24}	Ω_{25}
SCSC	0	0	0.2838	0.2879	0.3053	0.3062	0.3071	0.3112
		1	0.1558	0.1564	0.1594	0.161	0.167	0.1696
		2	0.1243	0.1247	0.1276	0.1303	0.1334	0.1355
		3	0.1083	0.1089	0.1114	0.113	0.1161	0.1176
		4	0.0984	0.0995	0.1016	0.1027	0.1057	0.1070
	1	0	0.2464	0.2597	0.2609	0.2629	0.264	0.2778
		1	0.1343	0.1347	0.1368	0.1389	0.1435	0.1464
		2	0.1082	0.1084	0.1113	0.1132	0.1164	0.1182
		3	0.0948	0.0958	0.0981	0.0991	0.1023	0.1036
		4	0.0869	0.0882	0.0901	0.0907	0.0939	0.0949
	2	0	0.2388	0.2451	0.2461	0.2489	0.2548	0.2618

Table 6 Continued...

BCs	$n_1 = n_2$	μ	The six dimensionless frequencies					
			Ω_{20}	Ω_{21}	Ω_{22}	Ω_{23}	Ω_{24}	Ω_{25}
		1	0.1278	0.1293	0.1297	0.1318	0.1361	0.1391
		2	0.1031	0.1033	0.1061	0.1078	0.1111	0.1128
		3	0.0906	0.0917	0.0939	0.0947	0.0979	0.0991
		4	0.0833	0.0847	0.0865	0.087	0.0901	0.0911
	10	0	0.2263	0.2271	0.2285	0.2296	0.2413	0.2438
		1	0.1190	0.1206	0.1228	0.1237	0.1266	0.1296
		2	0.0965	0.0969	0.0996	0.1010	0.1042	0.1058
		3	0.0853	0.0864	0.0885	0.0892	0.0924	0.0935
		4	0.0787	0.0802	0.0820	0.0823	0.0854	0.0863
CCCC	0	0	0.3000	0.3103	0.3267	0.3424	0.3489	0.3515
		1	0.1638	0.1676	0.1732	0.1782	0.1829	0.1834
		2	0.1289	0.1316	0.1361	0.1397	0.1425	0.1432
		3	0.1126	0.1145	0.1185	0.1216	0.1237	0.1244
		4	0.1027	0.1042	0.1079	0.1108	0.1126	0.1132
	1	0	0.2674	0.2675	0.2779	0.2912	0.2994	0.3186
		1	0.1413	0.1445	0.1496	0.1534	0.1581	0.1581
		2	0.1125	0.1147	0.1189	0.1217	0.1246	0.1248
		3	0.0991	0.1007	0.1044	0.1069	0.1091	0.1094
		4	0.0911	0.0924	0.0959	0.0981	0.1000	0.1003
	2	0	0.0331	0.0606	0.0757	0.1018	0.1094	0.1379
		1	0.0307	0.0505	0.0622	0.0769	0.0792	0.0983
		2	0.0288	0.0446	0.0546	0.0651	0.0661	0.0811
		3	0.0274	0.0407	0.0496	0.058	0.0585	0.0709
		4	0.0263	0.0378	0.046	0.0532	0.0534	0.0644
	10	0	0.2592	0.2592	0.2623	0.2747	0.2826	0.301
		1	0.1341	0.1372	0.1421	0.1456	0.1501	0.1502
		2	0.1073	0.1094	0.1134	0.116	0.1189	0.119
		3	0.0949	0.0964	0.1	0.1023	0.1045	0.1047
		4	0.0875	0.0887	0.0921	0.0942	0.0961	0.0963

Table 7 The first six frequencies of FGS square nanoplates (1-6-1) with $a/h = 50, K_1 = 45, K_2 = 20$.

BCs	$n_1 = n_2$	μ	The six dimensionless frequencies					
			Ω_{150}	Ω_{151}	Ω_{152}	Ω_{153}	Ω_{154}	Ω_{155}
SSSS	0	0	0.5337	0.5337	0.5339	0.5423	0.5423	0.5433
		1	0.2237	0.225	0.225	0.2267	0.2267	0.2271
		2	0.1651	0.1657	0.1657	0.1662	0.1662	0.1664
		3	0.1372	0.1372	0.1373	0.1373	0.1377	0.1377
		4	0.1196	0.1196	0.1197	0.1197	0.1200	0.1200
	1	0	0.4844	0.4995	0.4996	0.5076	0.5076	0.5085
		1	0.2094	0.2106	0.2106	0.2122	0.2122	0.2126
		2	0.1545	0.1551	0.1551	0.1555	0.1555	0.1557
		3	0.1284	0.1285	0.1285	0.1285	0.1288	0.1289
		4	0.1120	0.1120	0.1120	0.1120	0.1123	0.1124
	2	0	0.4741	0.4889	0.4890	0.4968	0.4968	0.4977
		1	0.2049	0.2061	0.2061	0.2077	0.2077	0.2081
		2	0.1512	0.1518	0.1518	0.1522	0.1522	0.1524
		3	0.1257	0.1257	0.1258	0.1258	0.1261	0.1261
		4	0.1096	0.1096	0.1097	0.1097	0.1100	0.1100
	10	0	0.4631	0.4775	0.4776	0.4853	0.4853	0.4862
		1	0.2002	0.2013	0.2013	0.2028	0.2028	0.2032
		2	0.1477	0.1483	0.1483	0.1487	0.1487	0.1489
		3	0.1228	0.1228	0.1228	0.1228	0.1232	0.1232
		4	0.107	0.107	0.1071	0.1071	0.1074	0.1074
CCCC	0	0	0.8159	0.8197	0.8197	0.8394	0.8394	0.8411
		1	0.273	0.2786	0.2786	0.2879	0.2879	0.2881
		2	0.2072	0.2075	0.2075	0.2104	0.2144	0.215

Table 7 Continued...

BCs	$n_1 = n_2$	μ	The six dimensionless frequencies					
			Ω_{150}	Ω_{151}	Ω_{152}	Ω_{153}	Ω_{154}	Ω_{155}
		3	0.1709	0.1746	0.1746	0.1766	0.1767	0.1767
		4	0.1497	0.1529	0.1529	0.1545	0.1545	0.1547
	1	0	0.7636	0.7672	0.7672	0.7856	0.7856	0.7872
		1	0.2555	0.2607	0.2607	0.2694	0.2695	0.2696
		2	0.1939	0.1942	0.1942	0.1969	0.2007	0.2012
		3	0.1599	0.1634	0.1634	0.1652	0.1654	0.1654
		4	0.1401	0.1431	0.1431	0.1446	0.1446	0.1448
	2	0	0.7474	0.7509	0.7509	0.7689	0.7689	0.7704
		1	0.2501	0.2551	0.2552	0.2636	0.2637	0.2639
		2	0.1898	0.1901	0.1901	0.1927	0.1964	0.1969
		3	0.1565	0.1599	0.1599	0.1617	0.1618	0.1618
		4	0.1371	0.14	0.1401	0.1415	0.1415	0.1417
	10	0	0.7300	0.7334	0.7334	0.7509	0.7510	0.7525
		1	0.2442	0.2491	0.2492	0.2574	0.2576	0.2577
		2	0.1853	0.1857	0.1857	0.1882	0.1919	0.1923
		3	0.1528	0.1562	0.1562	0.1579	0.1580	0.1581
		4	0.1339	0.1367	0.1368	0.1382	0.1382	0.1384

Thirdly, the impact of a/h ratio on the frequency of FGS square nanoplates for the first frequency, 15th frequency, 150th frequency, and 250th frequency are presented in Fig. 5. Observing that the frequency at all levels decreases when a/h increases from 10 to 50. Specifically, decreasing rapidly when a/h increases from 10 to 30, and gradually decreases when a/h takes values from 30 to 50. Besides, the nonlocal factor μ has little influence on the first frequency (Fig. 5a) but shows a clear influence at high frequencies (Fig. 5b-d). Furthermore, it can be seen that the nonlocal factor μ significantly affects the free vibration of FGS square nanoplates, especially at high frequencies.

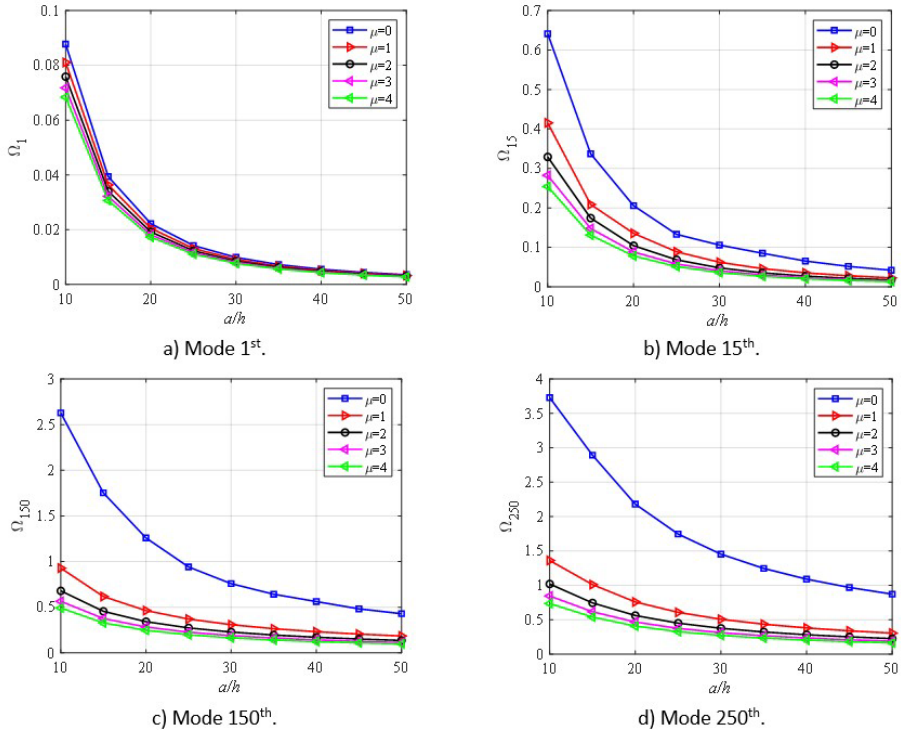

a) Mode 1st. b) Mode 15th.

c) Mode 150th. d) Mode 250th.

Figure 5 The impact of a/h on the frequencies of SSSS FGS square nanoplates (1-1-1) with $n_1 = n_2 = 1, K_1 = 50, K_2 = 5$.

Next, the effect of the power-law indexes $(n_1 = n_2)$ on the frequencies of the FGS square nanoplates are illustrated in Fig. 6. According to these figures, the frequency of FGS square nanoplates reduces when n_1 and n_2 increase for all low and high frequencies. Specifically, the frequency decreases rapidly as the power-law indexes increase from 0 to 2 and changes little with the power-law indexes greater than 2. It is observed that the local frequency significantly exceeds the nonlocal frequency of FGS square nanoplates, particularly at higher frequencies. This remarkable finding can be considered a new finding in this study.

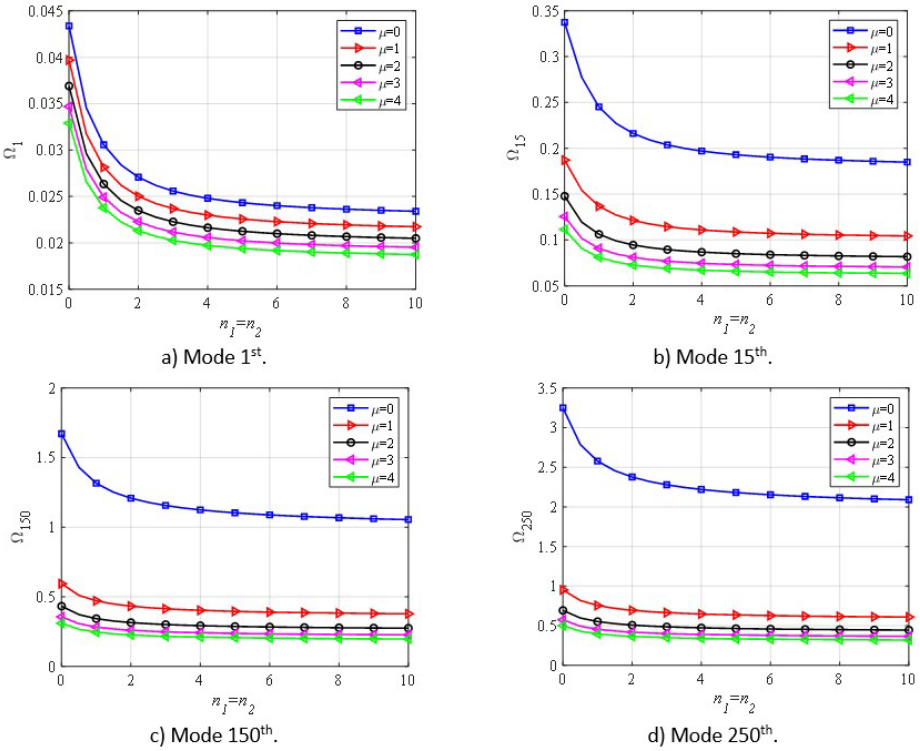

a) Mode 1st. b) Mode 15th.

c) Mode 150th. d) Mode 250th.

Figure 6 The effects of $(n_1 = n_2)$ on the frequencies of SCSC FGS square nanoplates (2-1-2) with $a/h = 20$, $K_1 = 25$, $K_2 = 10$.

Now, the influence of the schemes on the frequencies of FGS square nanoplates is illustrated in Fig. 7. Observing that when h_2/h ratio increases i.e., the ceramic core thickness increases, the frequencies of the FGS nanoplates increase for all sequence numbers. This is because the ceramic core thickness increases while the thickness of the two FGM skin layers reduces thus the FGS square nanoplate stiffness increases.

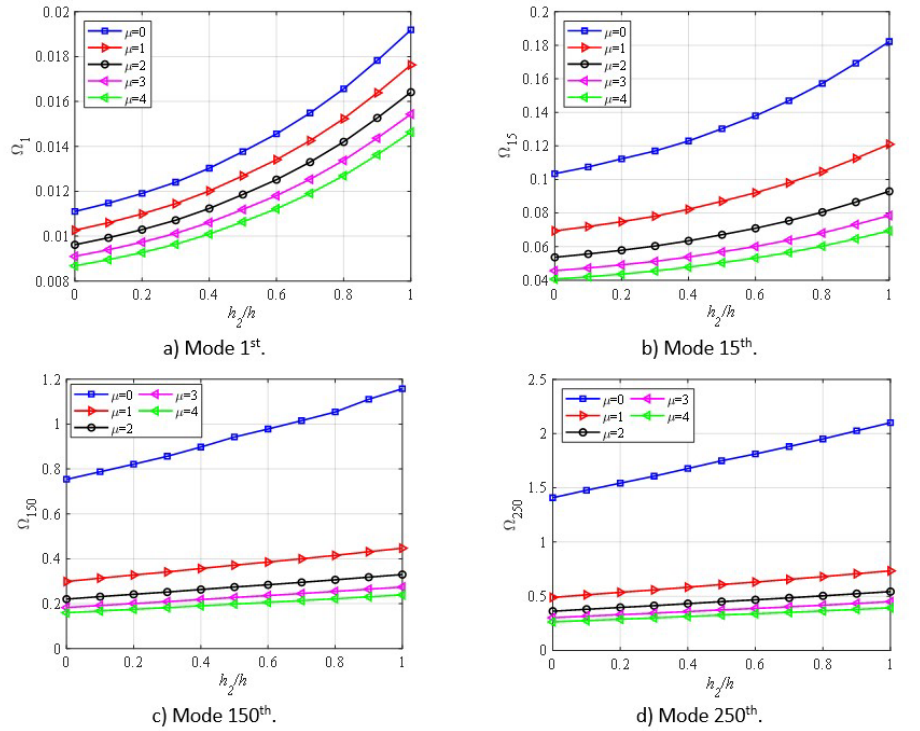

a) Mode 1st. b) Mode 15th.

c) Mode 150th. d) Mode 250th.

Figure 7 The effects of the schemes on the frequencies of SSSS FGS square nanoplates with $n_1 = n_2 = 2$, $K_1 = 15$, $K_2 = 5$.

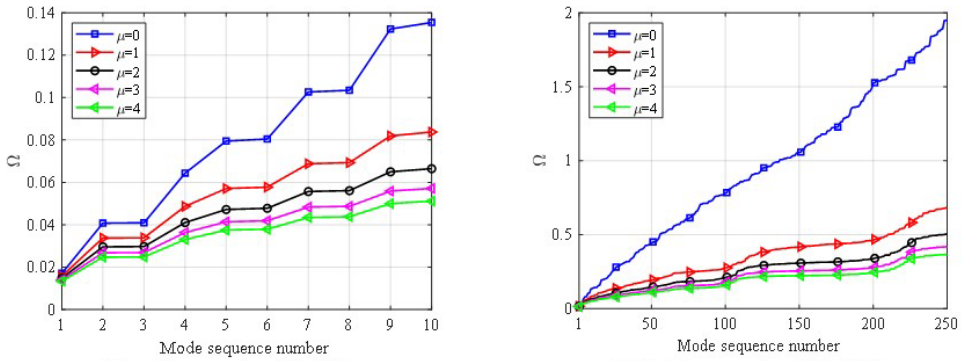

Figure 8 The effects of μ on free vibration of SSSS FGS nanoplates (1-8-1) with $a/h = 25, n_1 = n_2 = 2, K_1 = 15, K_2 = 5$.

In addition, the effects of μ on the mode sequence number are displayed in Figs. 8. As expected, the frequencies of the FGS square nanoplates increase with an increase in the mode sequence number. In addition, the frequencies in the case of the local plate (μ = 0) exhibit a more rapid increase compared to the nonlocal plates (μ > 0). It can also be observed that when μ > 0, the mode sequence number increases from 1 to 10 leading to an increase in the frequencies of nanoplates. However, the frequencies of FGS square nanoplates change little when the mode sequence number gets values from 50 to 250.

Furthermore, the effect of the foundation on the frequencies of FGS square nanoplates is demonstrated in Fig. 9. As can be seen, the EF helps increase the frequency of FGS square nanoplates for both low and high frequencies. The effects of the shear layer (K_2) is more positive than that of the spring layer (K_1). It can also be concluded that the spring layer (K_1) only affects the vibration of FGS square nanoplates at low frequencies but seems to have little impact at high frequencies.

Also, the influence of the spring layer (K_1) on the low frequencies are more significant than the high frequencies, while the shear layer (K_2) positively affects the free vibration of FGS square nanoplates at both low and high frequencies. This newly discovered result from the study holds valuable implications for the design, testing, and application of FGS square nanoplates in devices such as oscilloscopes and resonators.

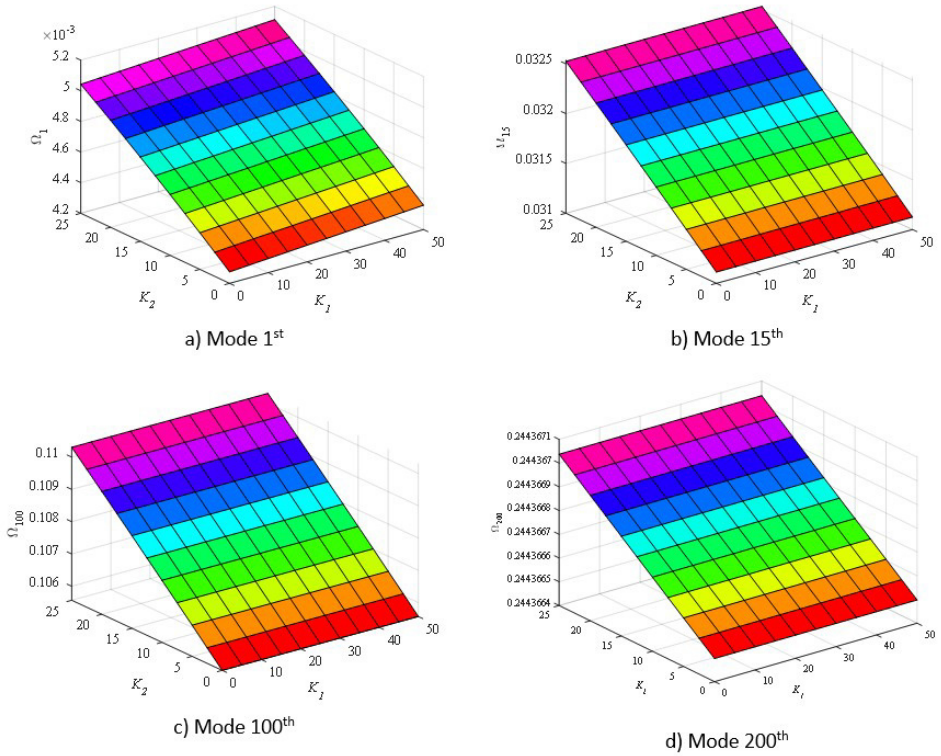

Figure 9 The influence of PF on the frequencies of SSSS FGS square nanoplates (1-1-1) with $a/h = 45, \mu = 1, n_1 = n_2 = 0.5$.

Finally, to confirm the advantages of the numerical method over the analytical method, the six high eigenmodes of the fully simply supported FGS circular and elliptical nanoplates are shown in Fig. 10 and Fig. 11, respectively.

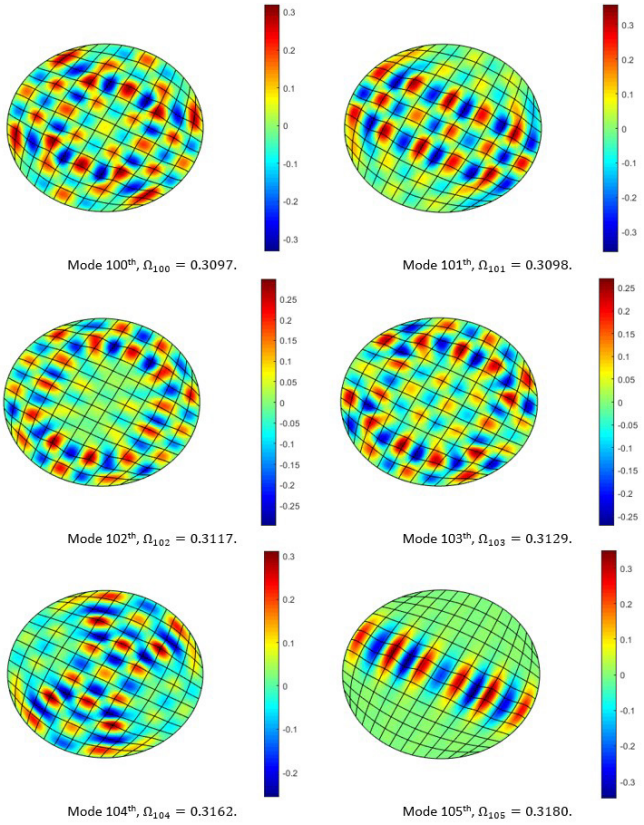

Figure 10 The six eigenmodes of the fully simply supported FGS circular nanoplate (1-2-2) with $R = 10$ nm, $h = R/15, \mu = 1, k_1 = k_2 = 1, K_1 = 10, K_2 = 5$.

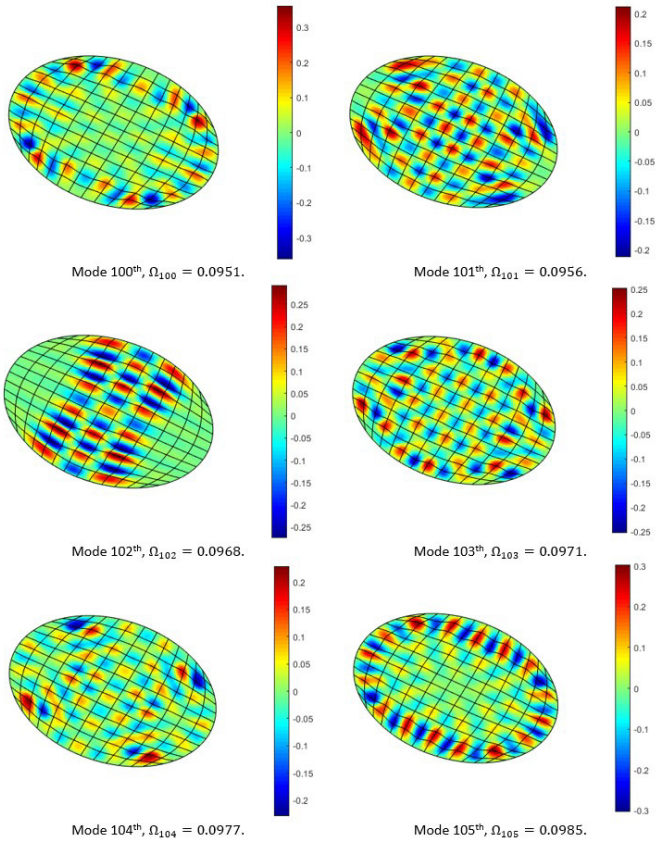

Figure 11 The six eigenmodes of the fully simply supported FGS elliptical nanoplate (1-2-1) with the semi-major axis $a = 10$ nm, the semi-minor axis $b = 3a/4, h = a/25, \mu = 2.5, k_1 = k_2 = 4, K_1 = 10, K_2 = 5$.

5 CONCLUSIONS

This study aims to analyze the high frequency analysis of FGS nanoplates (square, circular, elliptical) resting on PF by using higher-order IGA based on NET. Numerical examples and comments are made to illustrate in detail the influence of geometric parameters and material properties on the free vibrations of the FGS nanoplates, especially at high frequencies. Based on the obtained numerical results, some important observations can be summarized as follows:

- ➢ Using higher-order IGA eliminates the shear-locking correction factors, increases the convergence rate, improves accuracy and saves calculation time.
- ➢ Increasing the ceramic core thickness increases both the low and high frequencies of the FGS nanoplates.
- ➢ The power-law index increases reduce the FGS nanoplate stiffness, leading to a decrease in the frequencies of the FGS nanoplates at both low and high frequencies. Especially when power-law indexes increase from 0 to 2.
- ➢ The nonlocal factor diminishes the frequencies of FGS nanoplates, particularly at high frequencies. The impact of the nonlocal factor on high frequencies is more pronounced than its effect on low frequencies.
- ➢ Pasternak foundation increases the frequency of FGS nanoplates, specifically, the shear layer shows a greater influence than the spring layer, especially at high frequencies.
- ➢ The results obtained are expected to be useful for calculating, designing, and manufacturing nanoscale devices working at high frequencies in engineering practice.

Author's Contribuitions: Methodology, Validation, Formal analysis, Investigation, Writing Original draft, Le Hoai; Conceptualization, Writing - Reviewing & Editing, Supervision, Project administration, Nhan Thinh Hoang.

Editor: Rogério José Marczak

References

Ahmadi, I. (2022). Free vibration of multiple-nanobeam system with nonlocal Timoshenko beam theory for various boundary conditions. *Engineering Analysis with Boundary Elements, 143*, 719-739.

Aksencer, T., & Aydogdu, M. (2011). Levy type solution method for vibration and buckling of nanoplates using nonlocal elasticity theory. *Physica E: Low-dimensional Systems and Nanostructures, 43*(4), 954-959.

Ansari, E., & Setoodeh, A. (2020). Applying isogeometric approach for free vibration, mechanical, and thermal buckling analyses of functionally graded variable-thickness blades. *Journal of Vibration and Control, 26*(23-24), 2193-2209.

Ansari, E., Setoodeh, A., & Rabczuk, T. (2020). Isogeometric-stepwise vibrational behavior of rotating functionally graded blades with variable thickness at an arbitrary stagger angle subjected to thermal environment. *Composite Structures, 244*, 112281.

Arefi, M., & Zenkour, A. M. (2017). Thermo-electro-mechanical bending behavior of sandwich nanoplate integrated with piezoelectric face-sheets based on trigonometric plate theory. *Composite Structures, 162*, 108-122.

Baferani, A. H., Saidi, A., & Ehteshami, H. (2011). Accurate solution for free vibration analysis of functionally graded thick rectangular plates resting on elastic foundation. *Composite Structures, 93*(7), 1842-1853.

Banh-Thien, T., Dang-Trung, H., Le-Anh, L., Ho-Huu, V., & Nguyen-Thoi, T. (2017). Buckling analysis of non-uniform thickness nanoplates in an elastic medium using the isogeometric analysis. *Composite Structures, 162*, 182-193.

Borden, M. J., Scott, M. A., Evans, J. A., & Hughes, T. J. (2011). Isogeometric finite element data structures based on Bézier extraction of NURBS. *International Journal for Numerical Methods in Engineering, 87*(1-5), 15-47.

Cuong-Le, T., Nguyen, K. D., Lee, J., Rabczuk, T., & Nguyen-Xuan, H. (2021). A 3D nano scale IGA for free vibration and buckling analyses of multi-directional FGM nanoshells. *Nanotechnology, 33*(6), 065703.

Daikh, A. A., & Zenkour, A. M. (2020). Bending of functionally graded sandwich nanoplates resting on Pasternak foundation under different boundary conditions. *Journal of Applied and Computational Mechanics, 6*(Special Issue), 1245-1259.

Daikh, A. A., Drai, A., Bensaid, I., Houari, M. S. A., & Tounsi, A. (2021). On vibration of functionally graded sandwich nanoplates in the thermal environment. *Journal of Sandwich Structures & Materials, 23*(6), 2217-2244.

Daneshmehr, A., Rajabpoor, A., & Hadi, A. (2015). Size dependent free vibration analysis of nanoplates made of functionally graded materials based on nonlocal elasticity theory with high order theories. *International Journal of Engineering Science, 95*, 23-35.

Eringen, A. C. (1984). Plane waves in nonlocal micropolar elasticity. *International Journal of Engineering Science, 22*(8-10), 1113-1121.

Fleck, N., & Hutchinson, J. (1993). A phenomenological theory for strain gradient effects in plasticity. *Journal of the Mechanics and Physics of Solids, 41*(12), 1825-1857.

Hadji, L., Avcar, M., & Civalek, Ö. (2021). An analytical solution for the free vibration of FG nanoplates. *Journal of the Brazilian Society of Mechanical Sciences and Engineering, 43*(9), 418.

Hoa, L. K., Vinh, P. V., Duc, N. D., Trung, N. T., Son, L. T., & Thom, D. V. (2021). Bending and free vibration analyses of functionally graded material nanoplates via a novel nonlocal single variable shear deformation plate theory. *Proceedings of the Institution of Mechanical Engineers, Part C: Journal of Mechanical Engineering Science, 235*(18), 3641-3653.

Hughes, T. J., Cottrell, J. A., & Bazilevs, Y. (2005). Isogeometric analysis: CAD, finite elements, NURBS, exact geometry and mesh refinement. *Computer methods in applied mechanics and engineering, 194*(39-41), 4135-4195.

Jiang, Y., Li, L., & Hu, Y. (2023). A physically-based nonlocal strain gradient theory for crosslinked polymers. *International Journal of Mechanical Sciences, 245*, 108094.

Kachapi, S. H. (2020). Free vibration analysis of piezoelectric cylindrical nanoshell: nonlocal and surface elasticity effects. *WSEAS Transactions on Systems and Control, 15*, 141-165.

Le, P. B., & Tran, T.-T. (2023). Dynamic response of honeycomb-FGS shells subjected to the dynamic loading using non-polynomial higher-order IGA. *Defence Technology*.

Liew, K., He, X., & Wong, C. (2004). On the study of elastic and plastic properties of multi-walled carbon nanotubes under axial tension using molecular dynamics simulation. *Acta Materialia, 52*(9), 2521-2527.

Luat, D. T., Van Thom, D., Thanh, T. T., Van Minh, P., Van Ke, T., & Van Vinh, P. (2021). Mechanical analysis of bi-functionally graded sandwich nanobeams. *Advances in nano research, 11*(1), 55-71.

Natarajan, S., Chakraborty, S., Thangavel, M., Bordas, S., & Rabczuk, T. (2012). Size-dependent free flexural vibration behavior of functionally graded nanoplates. *Computational Materials Science, 65*, 74-80.

Nguyen, H. X., Nguyen, T. N., Abdel-Wahab, M., Bordas, S. P., Nguyen-Xuan, H., & Vo, T. P. (2017). A refined quasi-3D isogeometric analysis for functionally graded microplates based on the modified couple stress theory. *Computer Methods in Applied Mechanics and Engineering, 313*, 904-940.

Nguyen, V. P., Anitescu, C., Bordas, S. P., & Rabczuk, T. (2015). Isogeometric analysis: an overview and computer implementation aspects. *Mathematics and Computers in Simulation, 117*, 89-116.

Nguyen-Xuan, H., Tran, L. V., Thai, C. H., Kulasegaram, S., & Bordas, S. P. A. (2014). Isogeometric analysis of functionally graded plates using a refined plate theory. *Composites Part B: Engineering, 64*, 222-234.

Pham, Q.-H., Nguyen, P.-C., Tran, T. T., & Nguyen-Thoi, T. (2021). Free vibration analysis of nanoplates with auxetic honeycomb core using a new third-order finite element method and nonlocal elasticity theory. *Engineering with Computers*, 1-19.

Reddy, J. N. (2006). *Theory and analysis of elastic plates and shells*: CRC Press.

Rouhi, H., Ansari, R., & Darvizeh, M. (2016). Size-dependent free vibration analysis of nanoshells based on the surface stress elasticity. *Applied Mathematical Modelling, 40*(4), 3128-3140.

Shahsavari, D., Shahsavari, M., Li, L., & Karami, B. (2018). A novel quasi-3D hyperbolic theory for free vibration of FG plates with porosities resting on Winkler/Pasternak/Kerr foundation. *Aerospace Science and Technology, 72*, 134-149.

Shahverdi, H., & Barati, M. R. (2017). Vibration analysis of porous functionally graded nanoplates. *International Journal of Engineering Science, 120*, 82-99.

Sobhy, M. (2016). An accurate shear deformation theory for vibration and buckling of FGM sandwich plates in hygrothermal environment. *International Journal of Mechanical Sciences, 110*, 62-77.

Sobhy, M., & Radwan, A. F. (2017). A new quasi 3D nonlocal plate theory for vibration and buckling of FGM nanoplates. *International Journal of Applied Mechanics, 9*(01), 1750008.

Stölken, J. S., & Evans, A. (1998). A microbend test method for measuring the plasticity length scale. *Acta Materialia, 46*(14), 5109-5115.

Thai, C. H., Ferreira, A., Nguyen-Xuan, H., Nguyen, L. B., & Phung-Van, P. (2021). A nonlocal strain gradient analysis of laminated composites and sandwich nanoplates using meshfree approach. *Engineering with Computers*, 1-17.

Toupin, R. (1962). Elastic materials with couple-stresses. *Archive for rational mechanics and analysis, 11*(1), 385-414.

Touratier, M. (1991). An efficient standard plate theory. *International journal of engineering science, 29*(8), 901-916.

Zeighampour, H., & Shojaeian, M. (2019). Buckling analysis of functionally graded sandwich cylindrical micro/nanoshells based on the couple stress theory. *Journal of Sandwich Structures & Materials, 21*(3), 917-937.

Zemri, A., Houari, M. S. A., Bousahla, A. A., & Tounsi, A. (2015). A mechanical response of functionally graded nanoscale beam: an assessment of a refined nonlocal shear deformation theory beam theory. *Structural Engineering and Mechanics, An Int'l Journal, 54*(4), 693-710.

Zhu, C., Fang, X., Liu, J., Nie, G., & Zhang, C. (2022). An analytical solution for nonlinear vibration control of sandwich shallow doubly-curved nanoshells with functionally graded piezoelectric nanocomposite sensors and actuators. *Mechanics Based Design of Structures and Machines, 50*(7), 2508-2534.